Linear cortico-cortical mapping as a fundamental motif of brain connectivity organization

Jonathan F. O'Rawe and Hoi-Chung Leung

Stony Brook University

Integrative Neuroscience Program, Department of Psychology

Abstract

The pattern of region-to-region functional connectivity has major implications for understanding information transfer and transformation between brain regions. We extended connective field mapping to 3-dimensional anatomical space to derive estimates of cortico-cortical functional organization. For early visual regions we found that the topology of functional connectivity between early visual regions maintained a linear relationship along the anterior-posterior dimension, which is in agreement with the literature. For higher order visual regions (e.g. fusiform face area) our results revealed that their pattern of connectivity, the convergence and biased sampling, seem to contribute to some of their core receptive field properties. Further, we demonstrated that linearity of input is a fundamental aspect of functional connectivity of the whole cortex, with higher linearity between regions within a network than across networks. We found that the principle gradient of linearity resembles decompositions in both traditional functional connectivity and genetic expression reported in previous studies. In sum, the current work provides evidence supporting that linearity of input is likely a fundamental motif of functional connectivity between cortical regions for information processing and transfer, suggesting high linearity may preserve the integrity of information from one region to another within a network.

1. Introduction

One primary goal of systems neuroscience is to understand how integration occurs across cortical areas in order to support complex behavior (Cavada & Goldman-Rakic, 1991; Haber, Fudge, & McFarland, 2000; Hoover & Strick, 1993). Studies of brain connectivity, both anatomical and functional, have demonstrated some levels of spatially specific distributions between cortical regions. Different regions display specific patterns of long range and short range connections to target regions (Kravitz, Saleem, Baker, & Mishkin, 2011; Kravitz, Saleem, Baker, Ungerleider, & Mishkin, 2013; Van Essen & Gallant, 1994). It is believed that the properties of brain circuitry must provide a foundation of brain function and information processing, with pioneering work suggesting that connectivity profiles from one region to another allows for the potential understanding of information transfer/transformation. Topographic (linear), convergent, and divergent connectivity were postulated to support different computational needs of a specific neural network (Thivierge & Marcus, 2007). For example, systematic convergent connectivity in the visual hierarchy has been shown to be responsible for object processing, from lines (Hubel & Wiesel, 1962) to complex objects (Tanaka, 1997), while divergent connectivity has been theorized in motor systems for complex feedback mechanisms, such as motor efference copies (Wolpert & Flanagan, 2001).

Neuroimaging studies of brain connectivity, while indirect, has the benefit of its exhaustive sampling across the entire anatomical space, which complement the interpretations from the sparse sampling of rigorous anatomical tracing in animals. This is evident in resting state fMRI, where a low dimensional structure of large scale networks has been consistently found as a key organizational feature of the brain (Biswal et al., 2010; Di, Gohel, Kim, & Biswal, 2013; Fox et al., 2005; Yeo et al., 2011). Indeed, decomposing the the whole brain into it’s fundamental gradients have revealed a structure to this large scale network organization, with the primary gradient trending from unimodal networks to multimodal networks (Margulies et al., 2016). However, despite the overwhelming focus

on large scale brain organization, detailing the specific patterns of connectivity from one region to another remains a challenge. Here, we used a novel statistical modeling approach to examine the organization of functional connectivity across visual areas and the whole brian using restings-state fMRI data.

Topographic connectivity has been observed between early visual areas, which show retinotopic organization (Dumoulin & Wandell, 2008; Wang, Mruczek, Arcaro, & Kastner, 2015). Functional connectivity within a visual region, and between visual regions seem to follow along known eccentricity organization (Arcaro, Honey, Mruczek, Kastner, & Hasson, 2015). In other words, certain parts of a visual region that represent certain eccentricities are more likely to connect to the specific parts of other visual regions that represent similar eccentricities. While these investigations are possible in areas with a known and measurable sensory topology, a more general model, such as connective field mapping (Haak et al., 2013), is necessary for a more general study of connection topology. The connective field mapping technique fits 2 dimensional surface based population receptive fields (pRFs) using cortical signal from one region as the input to another region (Haak et al., 2013). This method has been used to model early visual areas, showing maintenance of retinotpic organization across them (Gravel et al., 2014; Haak et al., 2013).

It is unclear whether the linear pattern of connectivity observed in early visual cortex is dependent on a shared sensory topological organization, or whether it is present in any highly connected network. In theoretical models, spatial linearity in connectivity is postulated to serve the function of ensuring the fidelity of information transfer across a network (Thivierge & Marcus, 2007). Linear organization of connectivity also has the potential to generate complex abstract representations by virtue of topographic overlap (Tinsley, 2009). This suggests that abstract computations can be performed by biases in spatial connectivity and filtering between regions of a large scale network, in the same way that has been suggested in the visual system (Tinsley, 2009; Van Essen & Gallant, 1994).

In this study, we have modified and extended the connective field model, allowing for the estimation of linearity of functional connectivity between regions. This method fits a 3-D isotropic Gaussian to the connectivity pattern in the mapping region from individual voxels in the seed region (Fig. 1A). This fitting procedure produced four parameters, a 3-D location of the preferred locus of connectivity and a spread parameter, and acts like an encoding model for timecourses of BOLD activity (Fig. 1B). We further estimated the degree of linear mapping from one region to another by performing Procrustes analysis, fitting the spatial locations of the seed voxels with the estimated parameters from the 3-D connective field model. The degree to which these coordinates can be fit using a linear transformation provides the estimation of the linear mapping between them. We first examined the degree of linearity in the visual system, as the literature is relatively established, and then examined whether this is simply a specific case of a general motif of brain connectivity across various networks. We demonstrated high linearity in early visual regions, replicating prior work. We further showed when this linear motif breaks down in relation to higher order visual regions that are involved in complex filtering for representation of complex object categories. Finally, we found that linearity of input in visual regions is likely a special case of a connectivity motif found commonly throughout other major brain networks.

2. Results

2.1 Mapping Dorsal Visual Cortex connectivity in Ventral Visual Cortex

The 3-D connective field analysis revealed that dorsal and ventral portions of the visual cortex have an anterior-posterior organization in their functional connectivity. Figure 2A illustrates the group 3-D connective field maps in the ventral visual cortex for two voxels in the dorsal visual cortex. An animation of all seed voxels and their corresponding modeled Gaussian maps is available in the supplemental materials. Fig. 2B summarizes these results as a vector field in the seed region, with each vector from each voxel displaying the location of preferred connectivity as the relative displacement

from the center of the mapping region (Fig. 2B). Overall, the vector field showed a strong connectivity mapping along the predicted anterior-posterior organization, which was supported quantitatively by the high correlation between the seed's y-location and the mean modeled y-location of the Gaussian fit in the mapping region, with $r(394) = 0.71$, $p = 1.63 \times 10^{-62}$ ($r = 0.83$, with outliers removed). The standard deviation parameter of the Gaussian model also increased along the seed's y-axis (Fig. 2C left), which was supported quantitatively by the correlation between the seed's y-location and the modeled standard deviation parameter, with $r(394) = 0.61$, $p = 5.45 \times 10^{-42}$ (Fig 2C right). This relationship was further revealed between the dorsal and ventral portions of V1, V1, and V3, using a set of more restricted masks (Fig. 3). The Procrustes analysis yields an estimation of 42.36% linear organization for the highly inclusive masks of dorsal and ventral occipital cortex that spans multiple sub regions, while the linearity estimates were substantially higher for the selective masks: 68.79%, 67.45%, and 66.98% for V1, V2, and V3, respectively. These results together suggest that the inter-regional connectivity in early visual cortex mirrors the organization of eccentricity representation, with region to region connectivity ordered spatially along similar eccentricity locations, and the spread of that connectivity potentially following the increase in receptive field sizes in more anterior visual cortex.

To confirm the validity of our model, we examined the distribution of correlations between our predicted timecourses from the Gaussian model and the BOLD timecourses (see Fig. 1B) for each voxel in the large dorsal visual cortex mask (Fig. S1, left). The distribution of r-values across all subjects and all their correspond timecourses when using the matching prediction is strictly positive, with a mean of 0.55. While the distribution of correlations produced by nonmatched pairs is much wider with a mean of close to zero (Fig. S1, right).

2.2 Test-retest reliability of functional connectivity between early visual regions

We used the IBATRT dataset to assess the stability of the 3-D connective field model within individual subjects and across mean results for the dorsal and ventral visual cortex. For each subject,

the estimated y-location parameters from run 1 and run 2 were correlated across voxels (Fig. S2A). The distribution had a median of 0.60, demonstrating moderate to good reliability at the individual subject level. At the group level, the mean parameters for run 1 and run 2 correlated across voxels strongly, r = 0.98 (Fig. S2B).

In addition, we used the MSC data to test if reliability may further increase with increasing amount of scan time per subject. The median test-retest reliability within subjects increases with more scan time, with the 150 minutes in each split leading to a test-retest reliability of 0.81 (Fig. S2C). We then used each subject's data from all sessions (300 minutes) to generate a vector field for each individual, and showed that the anterior-posterior relationship is detectable in every subject (Fig. S3). Quantitatively, the correlation between y-location modeled Gaussian parameter and seed y-location was high: ranging form 0.5 to 0.72 across the 10 individuals.

Linearity estimates for the entire dorsal and ventral visual cortex for each MSC individual, albeit slightly lower, ranged between 28.81%-51.45%, which is around the group estimates calculated from the Cambridge-Buckner data. Similarly, linearity estimates of V1d→V2v were highly replicated in each MSC subject; they ranged from 54.50% to 70.37%.

2.3 FFA connectivity bias

Higher order visual regions have been characterized as complex filters (Van Essen & Gallant, 1994). This type of model has been successful in predicting FFA activation during a task (Kay & Yeatman, 2017). Here, we examined to what extent the region to region connectivity reflect this filtering process. We applied the 3-D connective field mapping method to model the pattern of right FFA connectivity with V1 and compared its connectivity profile with that of PPA, a region which is selective to stimuli that have more peripherally distinctive features. In comparison to the PPA, the FFA showed more connectivity with posterior V1. This was evident both across subjects (Fig. 4A, left), $t(197) = -4.92$, $p = 1.86 \times 10^{-6}$, and across voxels (Fig. 4A, center), $t(226) = -3.85$, $p = 1.55 \times 10^{-4}$.

In order to put the FFA's spatial pattern of connectivity with V1 in context with the prior results, we plotted the distribution of FFA-V1 connectivity against the dorsal visual cortex's distribution of connectivity with ventral visual cortex along the y-axis (Fig. 4A, right most plot, and Fig. 4B). This showed the more posteriorly oriented and convergent nature of the FFA's connectivity with V1. Indeed, the linearity estimate of V1 → FFA was substantially lower (7.23%) relative to connectivity among early visual regions (42.36%).

When an ideal model of V1 pRF organization was fed through the fitted model of connectivity between V1 and FFA, the FFA's pRF demonstrates a few classic hallmarks: a high degree of foveal representation, a larger receptive field, and even a slight bias towards the lower hemifield as seen in prior studies (Gomez et al., 2018; Kay et al., 2015) (Fig. 4C). While only nine of the voxels in the V1 model overlap with the central location of the pRFs in the FFA, comparing voxels in the FFA directly to voxels in V1 sharing the same eccentricity and angle showed on average a larger receptive field in the FFA, $t(154) = 11.15$, $p = 4.92 \times 10^{-21}$ (Fig. 4D). This suggests an integration across voxels of different pRF locations, rather than a simple selective connectivity with centrally located pRFs in V1.

2.4 Linearity of connectivity organization across the whole brain

While the early visual system demonstrated high linearity in connectivity between regions, a fundamental question left unanswered is whether this is a special property of the early visual cortex or it is a general motif of brain functional connectivity. To address this issue, we calculated the linearity of connectivity between all unique pairs of the 200 right hemisphere parcels in the Schaefer parcellation. For each subject of the MSC dataset, the distribution of linearity across the brain was shifted significantly to the right relative to the permutation null distribution (Fig. 5, top). The percentage of pairs for each subject that surpass the permutation $\alpha = .05$ ranges from 70.44 to 78.86% with the exception of two subjects at a lower value of 44.36% and 64.22%. Note that the outlier

MSC08 (with 44.36%) was identified by the original investigators to have a significant proportion of time in a drowsy state, affecting the reliability of this individual's BOLD data (Gordon et al., 2017).

Figure 5 illustrates the linear organization for three seed regions with other regions across the entire right hemisphere (Fig. 5, bottom). The flatmaps show a clear segregation of linearity values within and across the different networks, exemplified by seeding from anterior and posterior visual cortex demonstrating stronger linearity with different visual areas, and middle frontal gyrus demonstrating strong linearity with lateral prefrontal regions, and lower linearity between regions from different networks.

Further, nonmetric multidimensional scaling was applied to produce two dimensions that maximally reproduce the nonlinearity matrix (as a distance matrix) of the 200 parcels of right hemisphere (Fig. 6). We found that the primary mode to be similar to large scale whole brain decompositions observed in previous studies of normal functional connectivity and genetic expression data (Margulies et al., 2016; Murray et al., 2018). This mode scaled from lower order unimodal regions to higher order multimodal regions, with the negative end exemplified by visual and somatomotor networks and the positive end exemplified by default mode network. The second mode seems to be a fractionation of the primary mode, representing communication of information across these lower order/higher order boundaries.

3. Discussion

Using a 3-D Gaussian modeling approach with whole-brain resting-state fMRI data, we found that closely connected brain regions exhibit a relatively strong linear topology of their functional connectivity. This linear organization of region to region functional connectivity was highly reliable in early visual regions, following a topographic order along the anterior-posterior axis for eccentricity representation, as predicted by the literature (Arcaro et al., 2015; Gravel et al., 2014; Haak et al., 2013). In higher order visual areas we found that their connectivity profiles seemed to reflect their complex

filtering of information, such that FFA connectivity to V1 produced the hypothesized patterns of bias towards regions of V1 that have more foveal representations, and this connectivity bias was sufficient to reproduce the main features of FFA's pRF. In a whole brain analysis, linearity again appeared as a primary topographic organization for functional connectivity among regions within large-scale networks, including the default mode and frontoparietal networks, but weakened between regions across networks. Our overall findings thus suggest a ubiquitous nature of linearity of region to region communication among closely related functional regions in the human brain.

3.1 Eccentricity dependent connectivity in early visual cortex as a special case of linear communication

We found that the early visual cortex demonstrates orderly connectivity that maintains patterns of eccentricity representation across regions. This result replicates previous work that used resting state fMRI data and phase-locking fMRI task data in studying the regional topology of retinotopic organization (Arcaro et al., 2015; Gravel et al., 2014; Haak et al., 2013). The orderly functional connectivity likely contributes to the maintenance of retinotopic organization across the regions for visual processing. We also demonstrated that this motif breaks down for connectivity between early visual cortex and higher order visual cortices (Fig. 4). The pattern of FFA connectivity, its convergence and selection of foveal resources, predicts some fundamental aspects of the receptive field properties of this structure, which is specialized for face processing (Kanwisher, McDermott, & Chun, 1997). These findings on region-to-region connectivity patterns provide not only a structure for understanding what information is maintained across regions but also how the region may transform information and transfer the information to another region.

The linearity of connectivity observed in the early visual cortices seems to be a special case of a larger phenomenon. Our findings suggest that maintained spatial layout of information is a general mode of communication across the brain (Fig. 5, 6), likely at least partially for the purposes of high

fidelity information transmission across them (Thivierge & Marcus, 2007). In the visual cortex, synaptic selection driven by coincidental activity provides a potential mechanism for the generation and maintenance of this organization. However, activity dependent synaptic pruning is not the only mechanism that drives organization in early visual cortex, as a form of proto-organization driven by genetic expression and their products (e.g. morphogens) has been both demonstrated in animal models of development and evidence has been demonstrated for this in humans (Arcaro & Livingstone, 2017; Cheng, Nakamoto, Bergemann, & Flanagan, 1995). This mechanism of organization developing from molecular gradients is more general, pertaining to many brain systems. For example, this type of action has been shown to be responsible for organization of thalamocortical connections in and ordered spatial gradient, with Emx2 and Pax2 regulating the anterior-posterior organization of cortical fields and their thalamic afferents (Bishop, Goudreau, & O'Leary, 2000). We also found a strong linear organization from Area 46 to other lateral prefrontal cortex areas despite it's relatively weaker and less consistent retinotopy (Hagler & Sereno, 2006; Kastner et al., 2007). This in combination with gradients of genetic expression resembling our primary mode of linearity (Burt et al., 2018; Murray et al., 2018) suggests a link between linearity of input, genetics expression, and the large scale gradients of communication found in resting state fMRI.

3.2 Linearity and computation within and across brain networks

Spatial linearity of input-output allows for precise formation of input dependent action, such that each input can have an independent action (Thivierge & Marcus, 2007). Topographic organization and projections from topographic space has been postulated to produce ordered abstract space as shown in connectionist models (Tinsley, 2009). As it produces a continuous space of abstract relations, it affords complex information transformation in abstract space by the same general mechanism. This is the proposed mechanism underlying saliency map models, where information from many independent channels are combined topographically to represent the overall visual salience of an image (Itti &

Koch, 2000; Roggeman, Fias, & Verguts, 2010). These models have been successful in predicting eye movements to complex visual stimuli, attentional load responses in parietal cortex, and even working memory capacity (Foulsham & Underwood, 2008; Knops, Piazza, Sengupta, Eger, & Melcher, 2014).

With the simple assumption information is spatially segregated, a tractable form of general computation in the brain is through spatial biases in connectivity, which would subsume the above description of linearity. This would require multiple levels of observed spatial biases, with distinct information converging onto a neuron giving rise to many potential combinations of that information, and the exact combination being determined by spatial biases in convergence along the dendritic compartment (London & Häusser, 2005; Taylor, He, Levick, & Vaney, 2000). Therefore, each functional cortical column can be thought to represent a complex filter of the information transmitted to it via its connections (Van Essen & Gallant, 1994). In the visual cortex this can represent a feature in space, but it need not be so concrete. What do 'regions' compute, then? Or rather, what is the purpose of invoking a higher order regional computation (e.g. color perception)? Incoming sensory information is often both highly conflated and ambiguous. Perception of sensory information, such as visual information, is often highly dependent on context. Regional computation might be the form in which the brain solves this, with each voxel/column providing a complex filter for various features, and the combination of these in a stable state providing the end percept. This is akin to memory in Ising models of memory, such as traditional Hopfield network (Hopfield, 1982), with the exception that information is likely systematically ordered and graded, given our finding about linearity across the brain.

In general, the number of unique states of a computational system scales with the number of constituent parts (Hopfield, 1982). One testable prediction from this idea is that cortical specialization should increase in size as a generalization of an object category is learned. Object categorization seems to occur early in the feedforward processing stream, where learned categorization behavior is

independent of lateral prefrontal cortex (Minamimoto, Saunders, & Richmond, 2010). Indeed, this is more directly supported by the development of the FFA in children, as the area of activation increases in size as the object category is incidentally learned through development (Aylward et al., 2005; Golarai et al., 2007; Golarai, Liberman, & Grill-Spector, 2017; Golarai, Liberman, Yoon, & Grill-Spector, 2010), and experimentally in Greeble learning, a learning of an arbitrary object category (Gauthier & Tarr, 2002).

In this view of regional computation, linearity of input from one region to another may also provide a clue as to the similarity of feature space in one region in comparison to another, and therefore the similarity of the potential stable states. Previous work has examined this more directly, estimating linear transformations that map the representational dissimilarity matrices from one region to another (Basti et al., 2018). Our 3-D connective field model provides an appropriate description of the proposed mechanisms for these transformations, allowing for critical tests of this theory in our observational data.

3.3 Limitations and future directions

One general limitation for this type of analysis is parcel selection. Our estimations of linearity of connectivity between across regions likely were subjected to parcel selection. Given the multitude of parcellations and the multitude of methods used to obtain parcellations, the results could look slightly different if other justified parcellations were used. It's likely that our estimations of linearity would be stronger with "true" parcels, given that more appropriate specification in early visual cortex boosted our estimates of the linearity (from ~42% to ~68%). The 3-D Gaussian model itself has limitations and makes certain assumptions. For one, it assumes a single focal point of connectivity from one region to another, which is probably overly simplified. However, the final R^2 of the optimization procedure provides a marker for the fit of the model to the data; if these values are too low in the analysis, it would be inappropriate to make any conclusions about the fitted values. As the

R^2 of the model tended to increase with more scan time, a large proportion of the misfit is likely due to noise. With the 30 minute sessions of the MSC data, the modal responses tended around 0.30-0.60, indicating a reasonable fit. Gaussian mixture models can be developed in the future to account some conditions of misfit, such as regions with multiple maxima.

It is important to note that the 3-D connective field method has a high dependence on reliable signal in single voxels, as opposed to the more conventional analyses that either use signal averaging within ROIs or smoothing or both in order to increase SNR. Because of this, higher resolution datasets may suffer from less stability due to the increase of proportion of thermal noise in each voxel (Edelstein, Glover, Hardy, & Redington, 1986), though the impact on SNR can potentially be counterbalanced by a reduction in physiological noise (Bodurka, Ye, Petridou, Murphy, & Bandettini, 2007). Further studies are needed to test our approach on higher resolution data. Optimally, the goal is to achieve a reliable connective field mapping at the size of functional columns of the regions of interest, which may be feasible in the frontal cortex, where columns may be as large as 800-900 micron (Hirata & Sawaguchi, 2008; Masse, Hodnefield, & Freedman, 2017).

Integration of 3-D connectivity field information with computational models provides a new avenue for constraining and testing computational theories regarding brain dynamics. In addition, decomposing more selective groups of linearity matrices may give rise to another empirical method to discover different pathways of information processing.

3.3 Conclusions

We demonstrated empirically using resting-state fMRI data that linearity of functional connectivity is a common mode of communication across the cerebral cortex. This pattern of connectivity organization is higher within the same network, and illustrates a primary gradient comparable from two different data sources: resting-state functional connectivity and genetic expression. In sum, we showed that deriving finer scale (voxel level) organization of region to region

connectivity in volumetric space seems to be possible in resting-state fMRI data. Vector field representations of region to region connectivity has the potential to be an informative new metric to describe information transfer and transformation from one region to another, especially if the voxel size can be reduced to the size of a cortical column in the regions of interest.

4. Materials and Methods

4.1 Subjects

We used three publicly available datasets: one sample of healthy controls with well validated resting state fMRI data, which is the Cambridge Buckner subset of the 1000 functional connectomes project (Biswal et al., 2010), and two smaller samples inclined for test-retest reliability studies. The first small sample being the Intrinsic Brain Activity Test Retest (IBATRT) dataset (Zuo et al., 2014), and the second being the Midnight Scan Club (MSC) dataset (Gordon et al., 2017).

For the Cambridge Buckner data sample there were a total of 198 subjects (123 female), ages 18-30 (M = 21.03, SD = 2.31), with all subjects included in the final analysis. For the IBATRT data sample, there were a total of 36 subjects (18 female) ages 19-48 (M = 27.33, SD = 7.86) with two sessions and each with two runs. Four IBATRT subjects were excluded due to excessive motion in at least one of the four runs, leaving 32 subjects (16 female; ages 19-48, M = 26.03, SD = 7.24). For the MSC dataset, there were a total of 10 subjects (5 female), ages 24-34 (M = 29.1, SD = 3.3), and all included in the final analysis.

4.2 fMRI Parameters

Cambridge Buckner data (Siemens 3T Trim Trio): T1-weighted images were collected with MPRAGE with the following image parameters: slices = 192, matrix size = 144 x 192, voxel resolution = 1.20 x 1.00 x 1.33 mm^3. Resting state fMRI data were T2*-weighted images acquired using EPI with the following parameters: 47 interleaved axial slices, TR = 3000 ms, voxel resolution = 3.0 x 3.0 x 3.0 mm^3 (119 volumes).

IBATRT data (Siemens 3T Trim Trio): T1 weighted images were collected with MPRAGE with the following image parameters: slices = 176, matrix size = 256 x 256, voxel resolution = 1.0 x 1.0 x 1.0 mm^3. Resting state fMRI data were T2*-weighted images acquired using EPI with the following parameters: 29 ascending axial slices, slice gap = 0.36 mm, TR = 1750 ms, voxel resolution = 3.4 x 3.4 x 3.6 mm^3 (343 volumes each run). While there were up to 4 runs across 2 sessions for subjects, we only utilized the two runs in the first session.

MSC Data (Siemens 3T Trim Trio): Four T1 weighted images were collected: slices = 224, voxel resolution = 0.8 x 0.8 x 0.8 mm^3. Four T2 weighted images: 224 slices, voxel resolution 0.8 x0.8 x 0.8 mm^3. Resting state fMRI were T2* weighted images acquired using EPI: 36 interleaved axial slices, TR = 2200 ms, voxel resolution = 4 x 4 x 4 mm^3 (818 volumes each session). A gradient echo field map was collected with the same parameters as the BOLD EPI images for each session. There were 10 sessions for each subject, all utilized in the analysis.

4.3 Image Preprocessing

For each individual in the Cambridge Buckner and IBATRT data samples, preprocessing was performed utilizing SPM12 (http://www.fil.ion.ucl.ac.uk/spm/software/spm12/). The functional images were first corrected for slice timing, and then realigned to the middle volume according to a 6 parameter rigid body transformation. Structural images were coregistered with the mean functional image, segmented, and then normalized to the MNI template using both linear and nonlinear transformations. Functional images were normalized utilizing the same parameters as the structural normalization.

Further preprocessing was performed following the standard procedures of resting-state fMRI analysis either using CONN (Whitfield-Gabrieli & Nieto-Castanon, 2012) or custom Matlab scripts. A nuisance regression was constructed with the following confounding variables: 6 motion parameters up to their second derivatives, scans with evidence of excessive motion (Framewise Displacement [FD]

> .5 or DVARS > 5), session onset, estimated physiological signal generated through aCompCor (a temporal PCA of the white matter and CSF voxels with the number of components included determined individually on the basis of a Monte Carlo null model (Behzadi, Restom, Liau, & Liu, 2007)), and a linear drift component. For the Cambridge Buckner data the residuals from the nuisance regression were filtered utilizing a bandpass between the frequencies of 0.008 and 0.09 Hz, while for the IBATRT data, the band-pass filtering and nuisance regression were done simultaneously (Hallquist, Hwang, & Luna, 2013). Finally, the resultant data were despiked using a tangent squashing function.

For the MSC data, we utilized their release of preprocessed data which includes slice intensity correction, mode 1000 intensity normalization, realignment, transformation into Talairach space and FSL's field distortion correction (Smith et al., 2004). These data also came with additional preprocessing for resting-state analysis. Censored volumes were determined by an FD threshold of 0.2 mm. The data were first demeaned and detrended, then a nuisance regression was performed removing the following factors, with censored volumes ignored: global signal, white matter mean signal, CSF mean signal, and motion regressors with the full Volterra expansion. The data were then interpolated across the censored volumes using least squares spectral estimation followed by band-pass filtering between 0.009 and 0.08 Hz. The censored volumes were removed in the final resultant data samples for analysis (see Gordon et al., 2017 for full description of processing pipeline).

4.4 Regions of Interest

The initial analyses of 3-D connective field mapping were conducted using the visual areas as regions of interest (ROIs). For the early visual areas, we utilized the probabilistic visual atlas (Wang et al., 2015), selecting all voxels with any probability of either dorsal or ventral visual cortex, with no overlap between the two ROIs (see Fig. 2A). To determine whether the finding from the overall visual cortex mask was a general property of early visual areas, we also defined more selective masks of the dorsal and ventral portions of V1, V2, and V3, each with probability greater than 30% to reduce

overlap between the masks. We then applied the same connective field mapping analyses across each visual region's dorsal and ventral portions.

In an additional analysis, we created slightly more lenient V1 mask selecting any voxels that have a greater than 15% probability of being V1. We used this V1 ROI as a mapping region for the right fusiform face area (FFA) and the right parahippocampal place area (PPA), both FFA and PPA were derived using Neurosynth meta-analyses, with "faces" and "place" as keywords, respectively (Yarkoni, Poldrack, Nichols, Van Essen, & Wager, 2011).

For the whole brain linearity of connectivity analysis, we made use of a whole brain parcellation atlas of 400 regions. The parcels were generated by maximizing correlations within a parcel while minimizing local changes in correlations within a parcel (Schaefer et al., 2018). For time and computational feasibility, we only used the 200 parcels of the right hemisphere.

4.5 3-D Connective field Mapping and model parameters

For both the "seed" and "mapping" regions, the mean timecourse of the ROI was subtracted from each voxel's timecourse, so as to reduce the influence of correlation at the mean signal level, though in practice the results are similar with or without removing the means. Then, for each voxel within the "seed" region, we calculated its correlation with every voxel within the "mapping" region and transformed the resulting correlation values using Fisher's Z transformation. Each distribution of Fisher's Z values (for each seed voxel) was fitted with a 3-D isotropic Gaussian distribution (Fig. 1A):

$$g_v(x,y,z)=\frac{1}{\sigma^3(2\pi)^{3/2}}\exp-\frac{(x-x_0)^2+(y-y_0)^2+(z-z_0)^2}{2\sigma^2}$$

Initial values for the x_0, y_0, and z_0 parameters during the optimization procedure were the x, y, and z locations of the maximum Fisher's Z value, and and an arbitrarily small number (floating point epsilon) for the standard deviation. The optimization procedure had a lower bounds of the smallest location parameters within the mapping region and the floating point epsilon for the standard deviation, while

the upper bounds were the maximum location parameters and the smallest range of the 3 dimensions for the standard deviation. The parameters of the Gaussian were estimated by minimizing the correlation distance between the Fisher's Z values and the Gaussian probability density function using the interior-point algorithm (Byrd, Gilbert, & Nocedal, 2000), implemented by MATLAB's fmincon function (MathWorks Inc, 1995-2019). Predicted time-series for each voxel v in the seed region were estimated as the degree of overlap between the estimated Gaussian function and the activation pattern of the mapping region for each time-point t (Fig. 1B):

$$p_v(t) = \sum_x \sum_y \sum_z A(x, y, z, t) g_v(x, y, z)$$

Both the predicted time-series and the actual data time-series were z-scored to remove any arbitrary scaling factors. Fit was assessed by comparing the distribution of correlations between the each voxel's fitted model and the true data to the distribution of correlation between each voxel's true data and every other voxel's fitted model.

Finally, linearity of the connectivity from one region to another was estimated by fitting 3 space parameters of the Gaussian model to the 3 space parameters of the seed locations using Procrustes analysis (Kendall, 1989). The complement of the dissimilarity of the fit between the final output and the actual seed locations can be used as a direct measure of the degree of linearity of the mapping from one region to another. To visualize this transformation, a vector field can be created, with each vector originating at each seed voxel, and the orientation and length of the vector determined by the centered space parameters, it's preferred location in the mapping region in relation to the center of mass of the mapping region.

This 3-D connective field mapping analysis has been released in the form of a MATLAB toolbox, with a simple GUI wrapper to help guide analysis (www.nitrc.org/projects/r2r_prf/). This approach represents a simplification and extension of previous work.

We assessed test-retest reliability using the IBATRT and MSC datasets. For the IBATRT dataset, we examined the spatial correlation between the patterns of parameters in run 1 and run 2, within individual subjects and across session means. For the MSC dataset, we examined potential effects of added scan time to the the stability of the 3-D Gaussian parameters for individual subjects. We split the each subjects sessions into two groups, a test and a retest group. We varied the number of sessions in each group, with a maximum of 5 session per group, and calculated the test-retest reliability for each subject. We also performed 3-D connective field mapping for each subject with all their sessions to demonstrate the stability of the group effect at the level of individual subjects.

4.6 Deriving FFA pRF features from ideal V1 model

To study how the pRF features of the right FFA may be a result of biased connectivity from the primary visual cortex, we constructed an ideal model of pRFs in V1 on the basis of prior work in retinotopic mapping (Dumoulin & Wandell, 2008; Mackey, Winawer, & Curtis, 2017) with two orthogonal dimensions, one for eccentricity in the anterior-posterior dimension and one for angular representation in the dorsal-ventral dimension, with pRF size varying linearly in accordance to eccentricity. We then used the fitted 3-D connective field map from FFA (seed) to V1 (mapping) to produce a visual field response profile for each voxel within the FFA as a weighted mixture of the response profiles from the ideal V1 model. Then, we fit a 2-D Gaussian, using an analogous procedure to the 3-D connective field fitting, to each voxel's response profile to produce a pRF for each voxel within FFA.

4.7 Whole brain characterization of linearity of functional connectivity

We performed 3-D connective field mapping on each unique pair between all possible pairs out of the 200 parcels in the right hemisphere of the Shaefer atlas for each subject in the MSC data. For each fitted pair, we calculated the linearity of connectivity using Procrustes analysis. First, we tested whether or not the distribution of linearity across all pairs of parcels across the brain for each subject

were different than a permuted null distribution. This test was to demonstrate how typical linear relationships of connectivity are across the whole brain, and whether they can be generalized as a typical motif of inter-regional connectivity. We further selected several regions to test whether linearity is maintained through specific networks or generally across the brain.

Lastly, to compare with previous whole brain gradient decompositions (Margulies et al., 2016; Murray, Demirtaş, & Anticevic, 2018), we performed multidimensional scaling on the linearity matrices from all parcel pairs to estimate the primary and secondary gradients across the right hemisphere. The far ends of these gradients were considered to represent which regions maintain linear information across the brain. We produce a 2 dimensional solution, and visualized the gradients across the brain, demonstrating the potential top two modes of linear communication across the right hemisphere.

5. Conflicts of Interest

The authors disclose that there are no conflicts of interest relating to this work.

References

Arcaro, M. J., Honey, C. J., Mruczek, R. E., Kastner, S., & Hasson, U. (2015). Widespread correlation patterns of fMRI signal across visual cortex reflect eccentricity organization. *ELife*, *4*, e03952. https://doi.org/10.7554/eLife.03952

Arcaro, M. J., & Livingstone, M. S. (2017). A hierarchical, retinotopic proto-organization of the primate visual system at birth. *ELife*, *6*, e26196. https://doi.org/10.7554/eLife.26196

Aylward, E. H., Park, J. E., Field, K. M., Parsons, A. C., Richards, T. L., Cramer, S. C., & Meltzoff, A. N. (2005). Brain activation during face perception: evidence of a developmental change. *Journal of Cognitive Neuroscience*, *17*(2), 308–319.

Basti, A., Mur, M., Kriegeskorte, N., Pizzella, V., Marzetti, L., & Hauk, O. (2018). Analysing linear multivariate pattern transformations in neuroimaging data. *BioRxiv*, 497180. https://doi.org/10.1101/497180

Behzadi, Y., Restom, K., Liau, J., & Liu, T. T. (2007). A component based noise correction method (CompCor) for BOLD and perfusion based fMRI. *NeuroImage*, *37*(1), 90–101. https://doi.org/10.1016/j.neuroimage.2007.04.042

Bishop, K. M., Goudreau, G., & O'Leary, D. D. M. (2000). Regulation of Area Identity in the Mammalian Neocortex by Emx2 and Pax6. *Science*, *288*(5464), 344–349. https://doi.org/10.1126/science.288.5464.344

Biswal, B. B., Mennes, M., Zuo, X.-N., Gohel, S., Kelly, C., Smith, S. M., … Milham, M. P. (2010). Toward discovery science of human brain function. *Proceedings of the National Academy of Sciences*, *107*(10), 4734–4739. https://doi.org/10.1073/pnas.0911855107

Bodurka, J., Ye, F., Petridou, N., Murphy, K., & Bandettini, P. A. (2007). Mapping the MRI voxel volume in which thermal noise matches physiological noise—Implications for fMRI. *NeuroImage*, *34*(2), 542–549. https://doi.org/10.1016/j.neuroimage.2006.09.039

Burt, J. B., Demirtaş, M., Eckner, W. J., Navejar, N. M., Ji, J. L., Martin, W. J., … Murray, J. D. (2018). Hierarchy of transcriptomic specialization across human cortex captured by structural

neuroimaging topography. *Nature Neuroscience*, *21*(9), 1251. https://doi.org/10.1038/s41593-018-0195-0

Byrd, R. H., Gilbert, J. C., & Nocedal, J. (2000). A trust region method based on interior point techniques for nonlinear programming. *Mathematical Programming*, *89*(1), 149–185. https://doi.org/10.1007/PL00011391

Cavada, C., & Goldman-Rakic, P. S. (1991). Topographic segregation of corticostriatal projections from posterior parietal subdivisions in the macaque monkey. *Neuroscience*, *42*(3), 683–696. https://doi.org/10.1016/0306-4522(91)90037-O

Cheng, H.-J., Nakamoto, M., Bergemann, A. D., & Flanagan, J. G. (1995). Complementary gradients in expression and binding of ELF-1 and Mek4 in development of the topographic retinotectal projection map. *Cell*, *82*(3), 371–381. https://doi.org/10.1016/0092-8674(95)90426-3

Di, X., Gohel, S., Kim, E. H., & Biswal, B. B. (2013). Task vs. rest—different network configurations between the coactivation and the resting-state brain networks. *Frontiers in Human Neuroscience*, *7*. https://doi.org/10.3389/fnhum.2013.00493

Dumoulin, S. O., & Wandell, B. A. (2008). Population receptive field estimates in human visual cortex. *NeuroImage*, *39*(2), 647–660. https://doi.org/10.1016/j.neuroimage.2007.09.034

Edelstein, W. A., Glover, G. H., Hardy, C. J., & Redington, R. W. (1986). The intrinsic signal-to-noise ratio in NMR imaging. *Magnetic Resonance in Medicine*, *3*(4), 604–618. https://doi.org/10.1002/mrm.1910030413

Foulsham, T., & Underwood, G. (2008). What can saliency models predict about eye movements? Spatial and sequential aspects of fixations during encoding and recognition. *Journal of Vision*, *8*(2), 6–6. https://doi.org/10.1167/8.2.6

Fox, M. D., Snyder, A. Z., Vincent, J. L., Corbetta, M., Essen, D. C. V., & Raichle, M. E. (2005). The human brain is intrinsically organized into dynamic, anticorrelated functional networks. *Proceedings of the National Academy of Sciences*, *102*(27), 9673–9678. https://doi.org/10.1073/pnas.0504136102

Gauthier, I., & Tarr, M. J. (2002). Unraveling mechanisms for expert object recognition: Bridging brain activity and behavior. *Journal of Experimental Psychology: Human Perception and Performance*, *28*(2), 431–446. https://doi.org/10.1037//0096-1523.28.2.431

Golarai, G., Ghahremani, D. G., Whitfield-Gabrieli, S., Reiss, A., Eberhardt, J. L., Gabrieli, J. D. E., & Grill-Spector, K. (2007). Differential development of high-level visual cortex correlates with category-specific recognition memory. *Nature Neuroscience*. https://doi.org/10.1038/nn1865

Golarai, G., Liberman, A., & Grill-Spector, K. (2017). Experience Shapes the Development of Neural Substrates of Face Processing in Human Ventral Temporal Cortex. *Cerebral Cortex*, bhv314. https://doi.org/10.1093/cercor/bhv314

Golarai, G., Liberman, A., Yoon, J. M. D., & Grill-Spector, K. (2010). Differential development of the ventral visual cortex extends through adolescence. *Frontiers in Human Neuroscience*. https://doi.org/10.3389/neuro.09.080.2009

Gomez, J., Natu, V., Jeska, B., Barnett, M., & Grill-Spector, K. (2018). Development differentially sculpts receptive fields across early and high-level human visual cortex. *Nature Communications*, *9*(1). https://doi.org/10.1038/s41467-018-03166-3

Gordon, E. M., Laumann, T. O., Gilmore, A. W., Newbold, D. J., Greene, D. J., Berg, J. J., … Dosenbach, N. U. F. (2017). Precision Functional Mapping of Individual Human Brains. *Neuron*, *95*(4), 791-807.e7. https://doi.org/10.1016/j.neuron.2017.07.011

Gravel, N., Harvey, B., Nordhjem, B., Haak, K. V., Dumoulin, S. O., Renken, R., … Cornelissen, F. W. (2014). Cortical connective field estimates from resting state fMRI activity. *Frontiers in Neuroscience*, *8*. https://doi.org/10.3389/fnins.2014.00339

Haak, K. V., Winawer, J., Harvey, B. M., Renken, R., Dumoulin, S. O., Wandell, B. A., & Cornelissen, F. W. (2013). Connective field modeling. *NeuroImage*, *66*, 376–384. https://doi.org/10.1016/j.neuroimage.2012.10.037

Haber, S. N., Fudge, J. L., & McFarland, N. R. (2000). Striatonigrostriatal Pathways in Primates Form an Ascending Spiral from the Shell to the Dorsolateral Striatum. *Journal of Neuroscience*, *20*(6), 2369–2382.

Hagler, D. J., & Sereno, M. I. (2006). Spatial maps in frontal and prefrontal cortex. *NeuroImage*, *29*(2), 567–577. https://doi.org/10.1016/j.neuroimage.2005.08.058

Hallquist, M. N., Hwang, K., & Luna, B. (2013). The nuisance of nuisance regression: Spectral misspecification in a common approach to resting-state fMRI preprocessing reintroduces noise and obscures functional connectivity. *NeuroImage*, *82*, 208–225. https://doi.org/10.1016/j.neuroimage.2013.05.116

Hirata, Y., & Sawaguchi, T. (2008). Functional columns in the primate prefrontal cortex revealed by optical imaging in vitro. *Neuroscience Research*, *61*(1), 1–10. https://doi.org/10.1016/j.neures.2008.01.003

Hoover, J. E., & Strick, P. L. (1993). Multiple output channels in the basal ganglia. *Science*, *259*(5096), 819–821. https://doi.org/10.1126/science.7679223

Hopfield, J. J. (1982). Neural networks and physical systems with emergent collective computational abilities. *Proceedings of the National Academy of Sciences*, *79*(8), 2554–2558.

Hubel, D. H., & Wiesel, T. N. (1962). Receptive fields, binocular interaction and functional architecture in the cat's visual cortex. *The Journal of Physiology*, *160*(1), 106–154. https://doi.org/10.1113/jphysiol.1962.sp006837

Itti, L., & Koch, C. (2000). A saliency-based search mechanism for overt and covert shifts of visual attention. *Vision Research*, *40*(10), 1489–1506. https://doi.org/10.1016/S0042-6989(99)00163-7

Kanwisher, N., McDermott, J., & Chun, M. M. (1997). The fusiform face area: a module in human extrastriate cortex specialized for face perception. *The Journal of Neuroscience*, *17*(11), 4302–4311.

Kastner, S., DeSimone, K., Konen, C. S., Szczepanski, S. M., Weiner, K. S., & Schneider, K. A. (2007). Topographic Maps in Human Frontal Cortex Revealed in Memory-Guided Saccade and Spatial Working-Memory Tasks. *Journal of Neurophysiology*, *97*(5), 3494–3507. https://doi.org/10.1152/jn.00010.2007

Kay, K. N., Weiner, K. S., & Grill-Spector, K. (2015). Attention Reduces Spatial Uncertainty in Human Ventral Temporal Cortex. *Current Biology*, *25*(5), 595–600. https://doi.org/10.1016/j.cub.2014.12.050

Kay, K. N., & Yeatman, J. D. (2017). Bottom-up and top-down computations in word-and face-selective cortex. *Elife*, *6*, e22341.

Kendall, D. G. (1989). A Survey of the Statistical Theory of Shape. *Statistical Science*, *4*(2), 87–99. https://doi.org/10.1214/ss/1177012582

Knops, A., Piazza, M., Sengupta, R., Eger, E., & Melcher, D. (2014). A Shared, Flexible Neural Map Architecture Reflects Capacity Limits in Both Visual Short-Term Memory and Enumeration. *Journal of Neuroscience*, *34*(30), 9857–9866. https://doi.org/10.1523/JNEUROSCI.2758-13.2014

Kravitz, D. J., Saleem, K. S., Baker, C. I., & Mishkin, M. (2011). A new neural framework for visuospatial processing. *Nature Reviews Neuroscience*, *12*(4), 217–230. https://doi.org/10.1038/nrn3008

Kravitz, D. J., Saleem, K. S., Baker, C. I., Ungerleider, L. G., & Mishkin, M. (2013). The ventral visual pathway: an expanded neural framework for the processing of object quality. *Trends in Cognitive Sciences*, *17*(1), 26–49. https://doi.org/10.1016/j.tics.2012.10.011

London, M., & Häusser, M. (2005). Dendritic Computation. *Annual Review of Neuroscience*, *28*(1), 503–532. https://doi.org/10.1146/annurev.neuro.28.061604.135703

Mackey, W. E., Winawer, J., & Curtis, C. E. (2017). Visual field map clusters in human frontoparietal cortex. *Elife*, *6*, e22974.

Margulies, D. S., Ghosh, S. S., Goulas, A., Falkiewicz, M., Huntenburg, J. M., Langs, G., … Smallwood, J. (2016). Situating the default-mode network along a principal gradient of macroscale cortical organization. *Proceedings of the National Academy of Sciences*, *113*(44), 12574–12579. https://doi.org/10.1073/pnas.1608282113

Masse, N. Y., Hodnefield, J. M., & Freedman, D. J. (2017). Mnemonic Encoding and Cortical Organization in Parietal and Prefrontal Cortices. *The Journal of Neuroscience*, *37*(25), 6098–6112. https://doi.org/10.1523/JNEUROSCI.3903-16.2017

Minamimoto, T., Saunders, R. C., & Richmond, B. J. (2010). Monkeys Quickly Learn and Generalize Visual Categories without Lateral Prefrontal Cortex. *Neuron*, *66*(4), 501–507. https://doi.org/10.1016/j.neuron.2010.04.010

Murray, J. D., Demirtaş, M., & Anticevic, A. (2018). Biophysical Modeling of Large-Scale Brain Dynamics and Applications for Computational Psychiatry. *Biological Psychiatry: Cognitive Neuroscience and Neuroimaging*, *3*(9), 777–787. https://doi.org/10.1016/j.bpsc.2018.07.004

Roggeman, C., Fias, W., & Verguts, T. (2010). Salience maps in parietal cortex: Imaging and computational modeling. *NeuroImage*, *52*(3), 1005–1014. https://doi.org/10.1016/j.neuroimage.2010.01.060

Schaefer, A., Kong, R., Gordon, E. M., Laumann, T. O., Zuo, X.-N., Holmes, A. J., … Yeo, B. T. T. (2018). Local-Global Parcellation of the Human Cerebral Cortex from Intrinsic Functional Connectivity MRI. *Cerebral Cortex*, *28*(9), 3095–3114. https://doi.org/10.1093/cercor/bhx179

Smith, S. M., Jenkinson, M., Woolrich, M. W., Beckmann, C. F., Behrens, T. E. J., Johansen-Berg, H., … Matthews, P. M. (2004). Advances in functional and structural MR image analysis and implementation as FSL. *NeuroImage*, *23*, S208–S219. https://doi.org/10.1016/j.neuroimage.2004.07.051

Tanaka, K. (1997). Mechanisms of visual object recognition: monkey and human studies. *Current Opinion in Neurobiology*, *7*(4), 523–529.

Taylor, W. R., He, S., Levick, W. R., & Vaney, D. I. (2000). Dendritic Computation of Direction Selectivity by Retinal Ganglion Cells. *Science*, *289*(5488), 2347–2350. https://doi.org/10.1126/science.289.5488.2347

Thivierge, J.-P., & Marcus, G. F. (2007). The topographic brain: from neural connectivity to cognition. *Trends in Neurosciences*, *30*(6), 251–259. https://doi.org/10.1016/j.tins.2007.04.004

Tinsley, C. J. (2009). Creating abstract topographic representations: Implications for coding, learning and reasoning. *Biosystems*, *96*(3), 251–258. https://doi.org/10.1016/j.biosystems.2009.03.003

Van Essen, D. C., & Gallant, J. L. (1994). Neural mechanisms of form and motion processing in the primate visual system. *Neuron*, *13*(1), 1–10.

Wang, L., Mruczek, R. E. B., Arcaro, M. J., & Kastner, S. (2015). Probabilistic Maps of Visual Topography in Human Cortex. *Cerebral Cortex*, *25*(10), 3911–3931. https://doi.org/10.1093/cercor/bhu277

Whitfield-Gabrieli, S., & Nieto-Castanon, A. (2012). Conn: A Functional Connectivity Toolbox for Correlated and Anticorrelated Brain Networks. *Brain Connectivity*, *2*(3), 125–141. https://doi.org/10.1089/brain.2012.0073

Wolpert, D. M., & Flanagan, J. R. (2001). Motor prediction. *Current Biology*, *11*(18), R729–R732. https://doi.org/10.1016/S0960-9822(01)00432-8

Yarkoni, T., Poldrack, R. A., Nichols, T. E., Van Essen, D. C., & Wager, T. D. (2011). Large-scale automated synthesis of human functional neuroimaging data. *Nature Methods*, *8*(8), 665–670. https://doi.org/10.1038/nmeth.1635

Yeo, B. T. T., Krienen, F. M., Sepulcre, J., Sabuncu, M. R., Lashkari, D., Hollinshead, M., … Buckner, R. L. (2011). The organization of the human cerebral cortex estimated by intrinsic functional connectivity. *Journal of Neurophysiology*, *106*(3), 1125–1165. https://doi.org/10.1152/jn.00338.2011

Zuo, X.-N., Anderson, J. S., Bellec, P., Birn, R. M., Biswal, B. B., Blautzik, J., … Milham, M. P. (2014). An open science resource for establishing reliability and reproducibility in functional connectomics. *Scientific Data*, *1*, 140049. https://doi.org/10.1038/sdata.2014.49

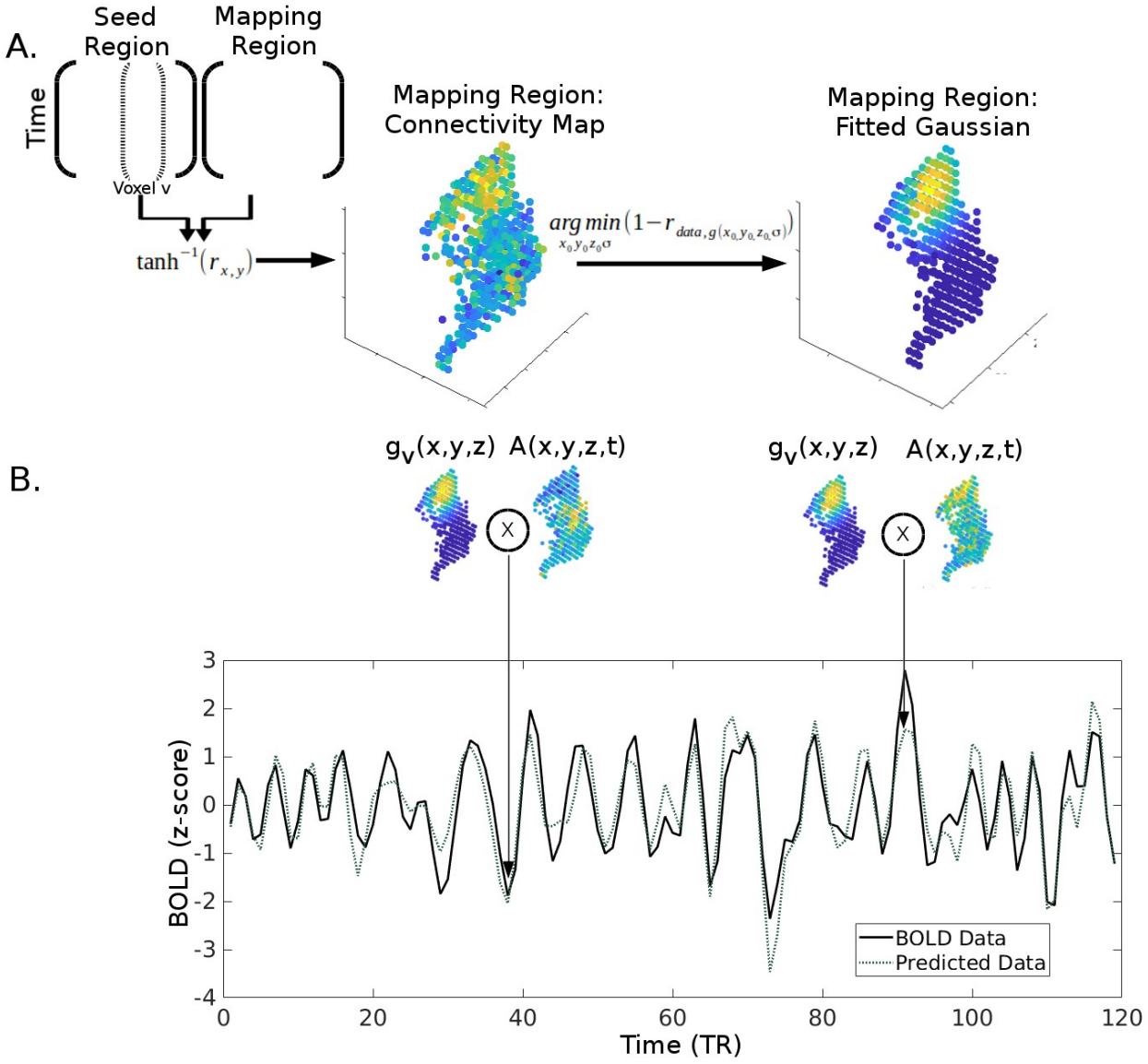

Figure 1: 3D Connective Field Modeling. **(A)** Gaussian fitting procedure. Each seed voxel's timecourse (dotted bracket inside the matrix on the left represents the timecourse of one voxel of the seed region) is correlated to every voxel's timecourse in the mapping region and then Fisher's z transformed. For each seed voxel, the corresponding 3-D Fisher's Z matrix is then fitted to the 3 dimensional Gaussian model, by minimizing the correlation distance between the Fisher's Z matrix and the Gaussian distribution. The fitted Gaussian parameters, location and standard deviation parameters, for each seed voxel are used in subsequent quantitative tests. **(B)** Time-series prediction model. For

each time-point, the overlap between the actual activation in the mapping region [A(x,y,z,t)] and the fitted Gaussian distribution in the mapping region [$g_v(x,y,z)$] for that particular seed voxel produce the expected level of activity in the corresponding seed voxel. This procedure was used to evaluate goodness of the Gaussian fit.

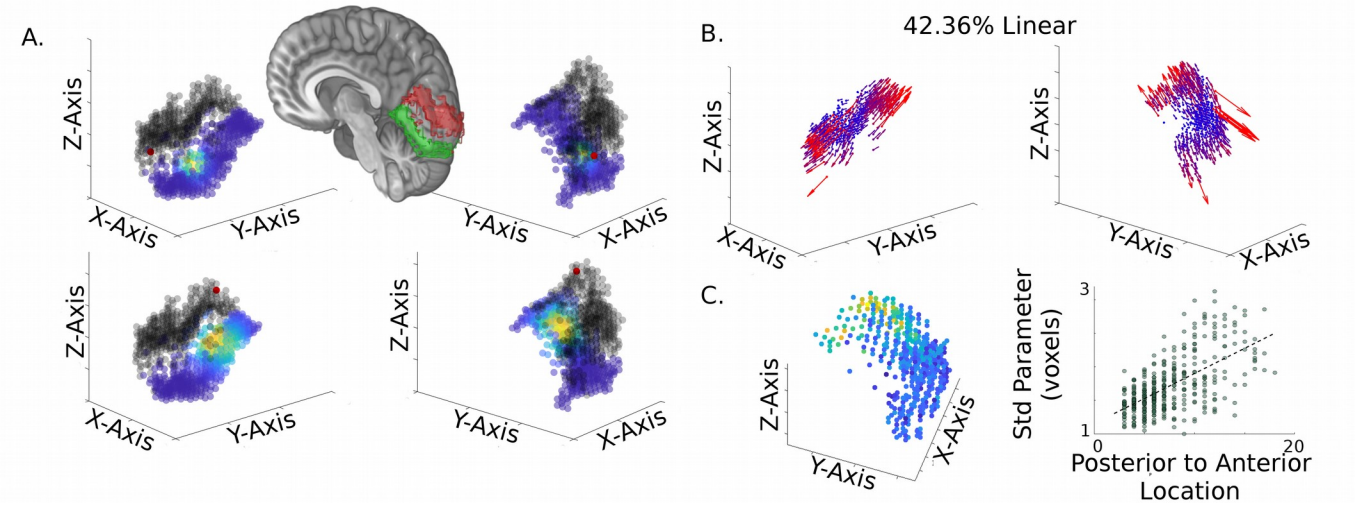

Figure 2: Group results of the 3-D connective field modeling in dorsal visual cortex and the ventral visual cortex using the Cambridge Buckner sample of resting-state fMRI data. **(A)** Examples of the resulting Gaussian model are shown for two seed voxels (red dots), plotted in red among other voxels (black circles) in dorsal visual cortex (red mask), and their associated group level Gaussian fit (colored from blue to yellow) in ventral visual cortex (green mask). The two columns show the same data rotated by 180 degrees from eachother for full visualization. Full animation can be found in Supplementary materials. **(B)** Preferred location of connectivity of each seed voxel is plotted as a vector with the origin in the seed location, and the vector direction showing the fitted x_0 y_0 and z_0 parameters. The vectors are colored coded with blue to red representing low to high euclidean norm of the vector. **(C)** Group results of the Gaussian model's standard deviation parameter. **(A)** Each voxel of the seed region, dorsal visual cortex, is plotted with each voxel's data point's color representing by the standard deviation of their connective field model. Warmer colors represent larger standard deviations, while colder colors represent smaller standard deviations. **(B)** This plot shows the correlation between the anterior-posterior extent of the seed voxel and their associated standard deviation parameter, suggesting that standard deviation increases along more anterior voxels.

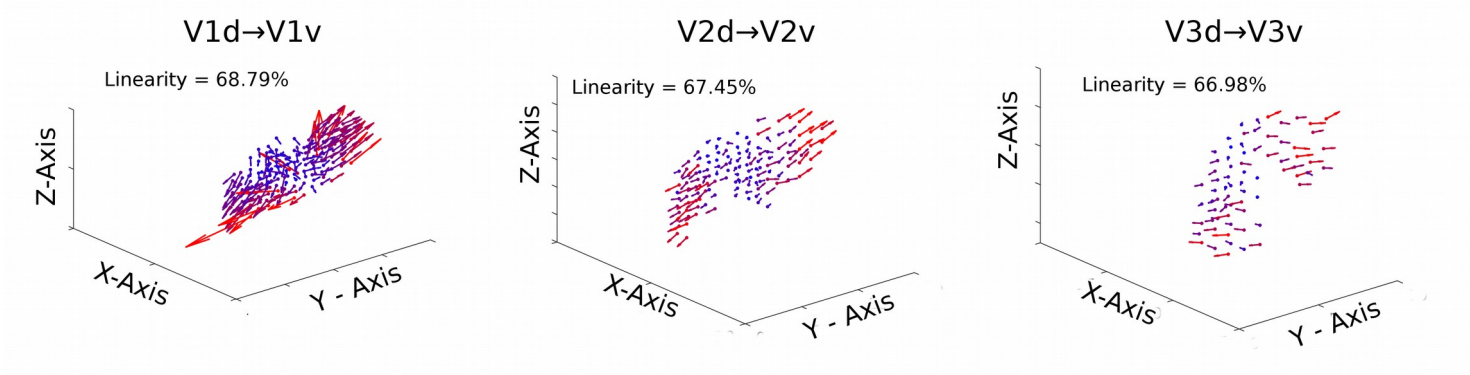

Figure 3: The linear organization pattern of region-to-region functional connectivity is similar across early visual areas. More constrained ROI masks were selected to demonstrate that the connectivity patterns from dorsal to ventral portions of V1-V3 are constrained by the anterior-posterior axis, likely along the topographic eccentricity representation. The vector fields are visualized similarity as described in Figure 2, with the red-blue color scale representing the euclidean norm of each seed voxel's vector.

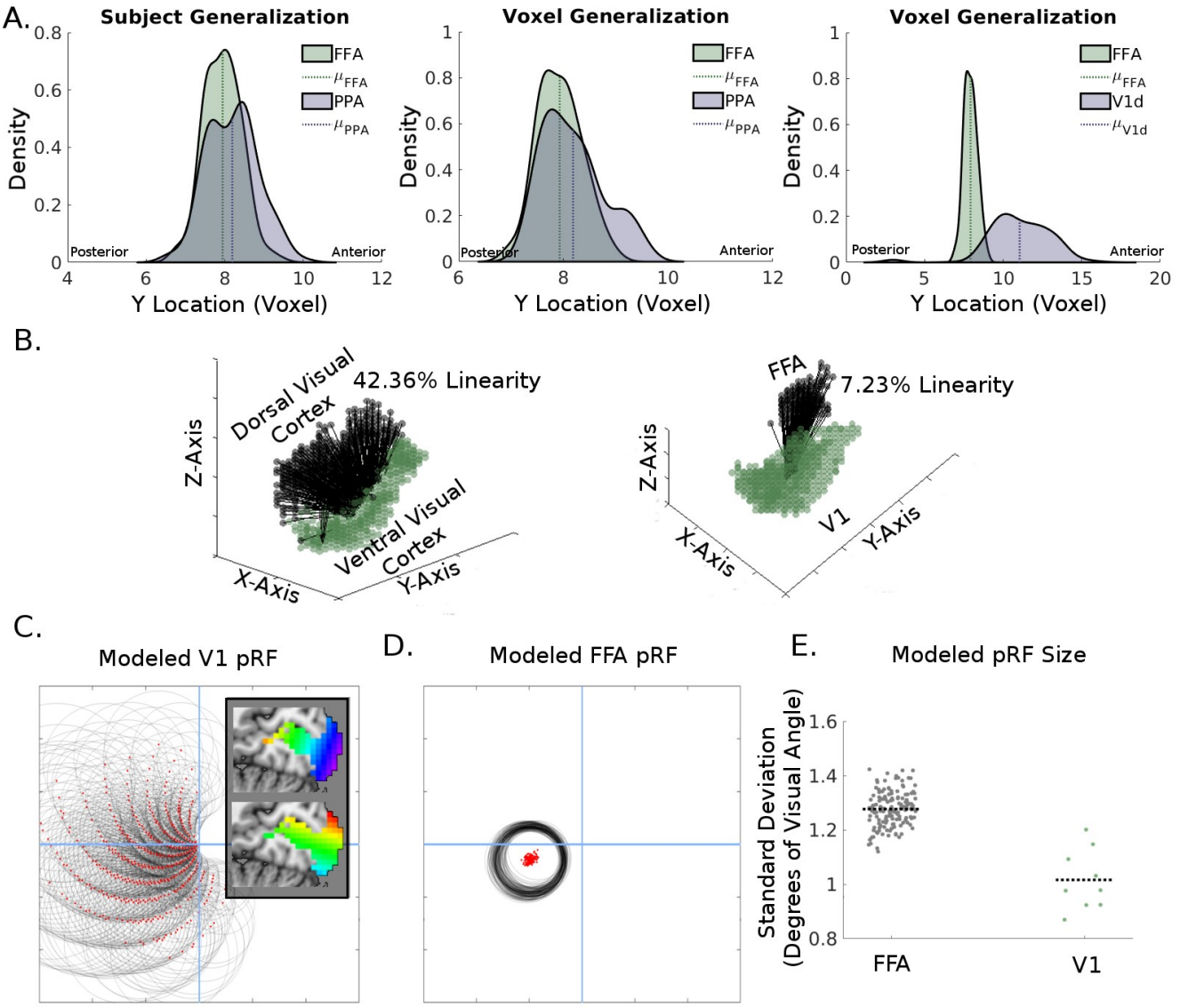

Figure 4: Pattern of connectivity between FFA and V1 corresponds well with FFA's more central/foveal pRF observed in previous studies. **(A)** As shown across subjects (left) and across voxels (right), compared to the PPA, FFA showed a more posteriorly located and narrower range of connectivity with V1. For comparison, the distribution of Y Location parameters for the FFA to V1 model is plotted against the dorsal visual cortex to ventral visual cortex model (right). **(B)** Another representation of the connectivity biases in FFA to V1 (right) in comparison to dorsal and ventral visual cortex (left). The black points represent voxels within the seed region and the green voxels within the mapping region

and the vectors connecting them represent the seed voxels' preferred connectivity location along the mapping region. Note the relatively higher amount of convergent connectivity from FFA to V1 and much lower linearity. **(C)** Using a ideal model of V1 organization, with 2 orthogonal axes representing eccentricity and angle (see inset), we show that applying the group fitted region to region pRF mapping the V1 from the FFA, we can reproduce some important qualities of FFA's pRF, such as a more central representation **(D)** and quantitatively larger pRFs **(E)**. Plots shown in **(C,D)** are visualized similarly as in previous studies (Kay et al., 2015) with red dots representing the center of the pRFs and the gray circles representing the standard deviation of the pRFs, plotted on the 4 quadrants of visual space. As the ROIs are in the right hemisphere, the pRFs of the seed voxels show lateralized representation of the left visual space.

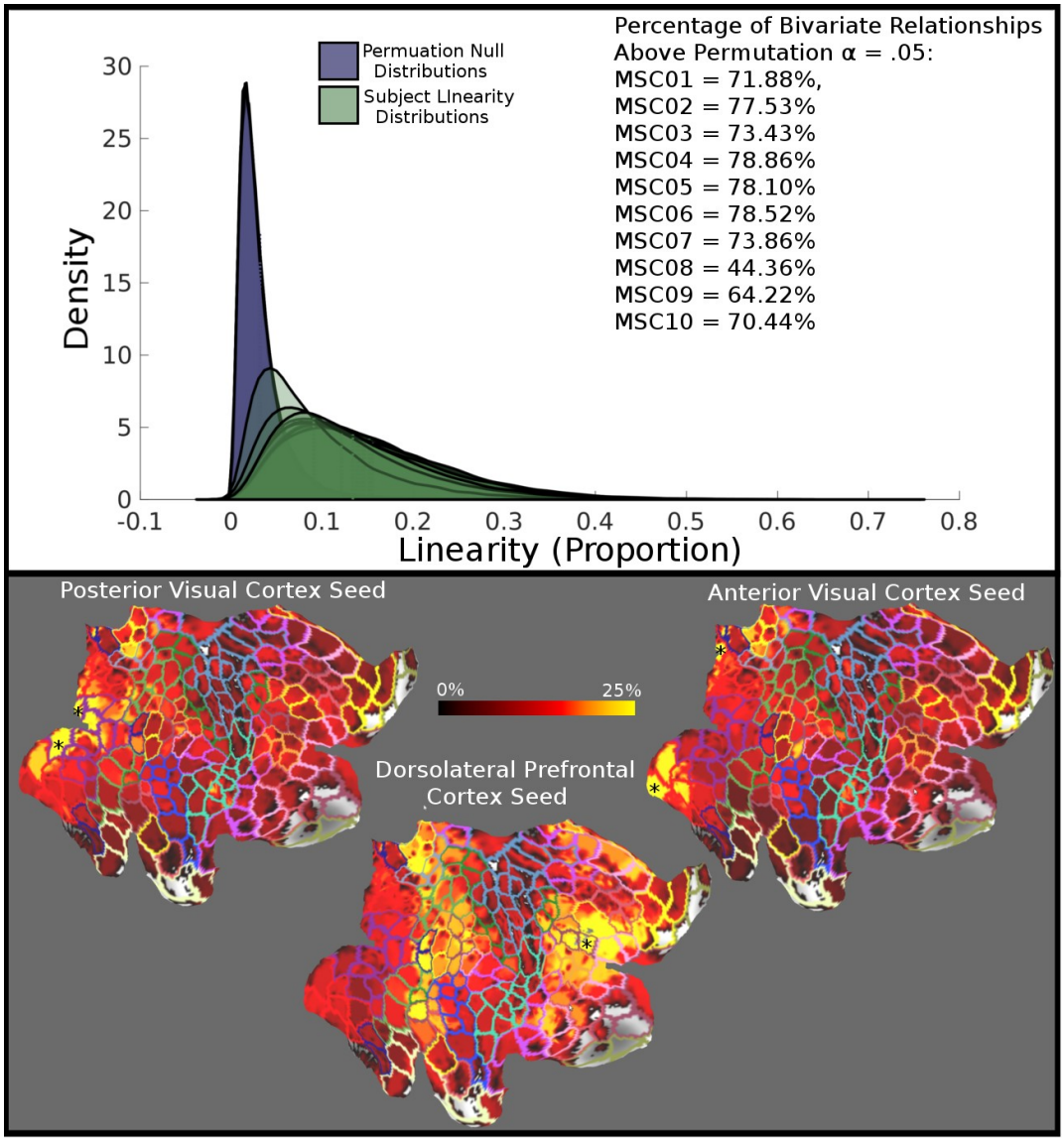

Figure 5: Linearity of input is a general rule of functional connectivity. **(TOP)** Each MSC subject's distribution of linearity estimates is plotted against their own permutation null distribution. All subjects showed a large proportion of bivariate relationships that are of greated linearity than would be expected due to chance. **(BOTTOM)** Mean linearity estimates are shown from 3 seed regions, posterior visual cortex, anterior visual cortex, and dorsolateral prefrontal cortex. The color scale from warmer to cooler represents higher to lower linearity for the seed regions' connective field in the other brain regions. This whole brain illustration demonstrates that while linearity is a general phenomenon for region-to-

region connectivity, it is maintained within specific networks, suggesting function in maintaining integrity of information transfer across regions within a network.

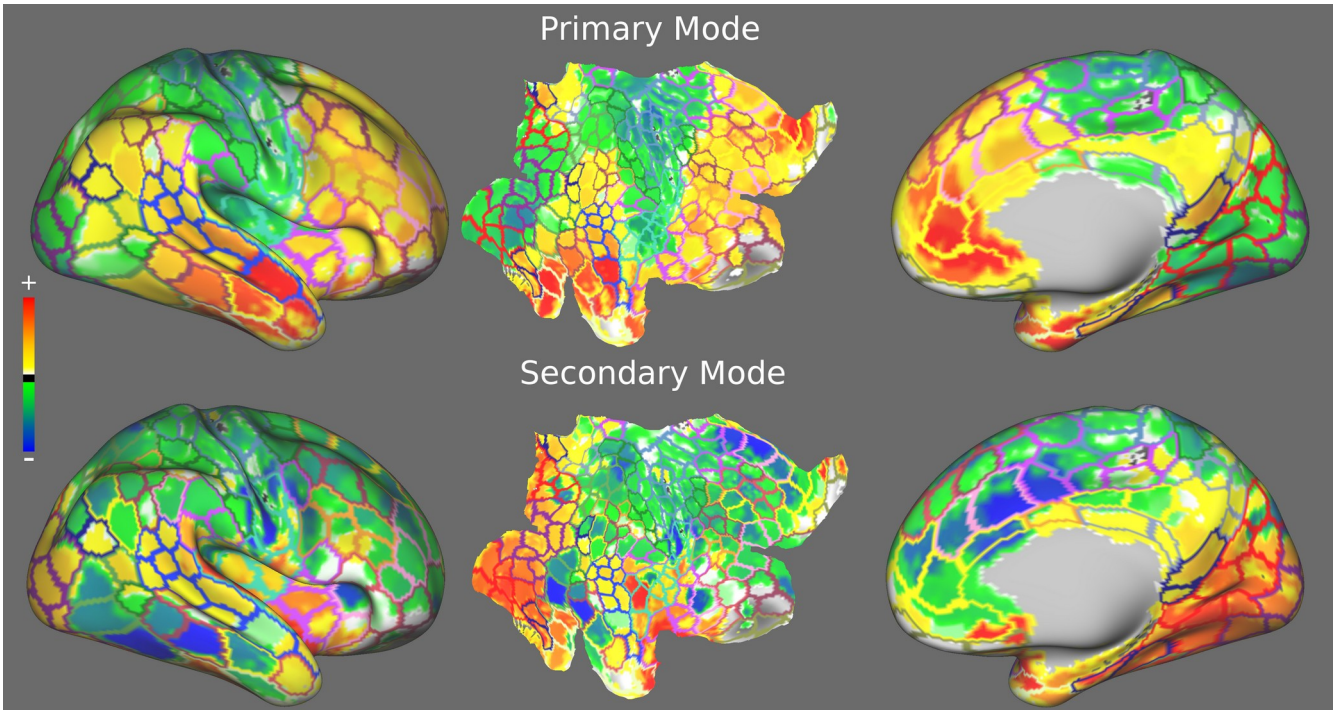

Figure 6: Gradient decomposition of whole brain linearity. Whole brain region-to-region linearity matrix was decomposed using nonmetric multidimensional scaling in order to examine organizational patterns of linearity across the brain. The gradients are color scaled from red to blue, with red colors representing one side of the gradient, and blue colors representing the other side of the gradient. **(TOP)** Primary mode, demonstrates a segregation of higher order to lower order brain region. **(BOTTOM)** Second mode, the fractionated nature suggests integration of information across higher order and lower order cortex.